Nuclear Engineering and Technology 53 (2021) 637–646

Contents lists available at ScienceDirect

Nuclear Engineering and Technology

journal homepage: www.elsevier.com/locate/net

Original Article

Design and analysis of a free-piston stirling engine for space nuclear power reactor

Zhiwen Dai, Chenglong Wang*, Dalin Zhang**, Wenxi Tian, Suizheng Qiu, G.H. Su

School of Nuclear Science and Technology, Shanxi Engineering Research Center of Advanced Nuclear Energy, State Key Laboratory of Multiphase Flow in Power Engineering, Xi'an Jiaotong University, Xi'an 710049, China

ARTICLE INFO

Article history:
Received 16 January 2020
Received in revised form
2 July 2020
Accepted 10 July 2020
Available online 21 July 2020

Keywords:
Space nuclear power reactor
Free-piston Stirling engine
Improved simple adiabatic analysis
Design and analysis

ABSTRACT

The free-piston Stirling engine (FPSE) has been widely used in aerospace owing to its advantages of high efficiency, high reliability, and self-starting ability. In this paper, a 20-kW FPSE is proposed by analyzing the requirements of space nuclear power reactor. A code was developed based on an improved simple analysis method to evaluate the performance of the proposed FPSE. The code is benchmarked with experimental data, and the maximum relative error of the output power is 17.1%. Numerical results show that the output power is 21 kW, which satisfies the design requirements. The results show that: a) reducing the pressure shell's thickness can improve the output power significantly; b) the system efficiency increases with the wire porosity, while the growth of system efficiency decreases when the porosity is higher than 80%, and system efficiency exhibits a linear relationship with the temperatures of the cold and hot sides; c) the system efficiency increases with the compression ratio; the compression ratio increases by 16.7% while the system efficiency increases by 42%. This study can provide valuable theoretical support for the design and analysis of FPSEs for space nuclear power reactors.

1. Introduction

Given the increasing demand for space exploration and the limitations of solar and chemistry batteries for deep space or planetary surface missions, space nuclear power reactors with high efficiency, power, and reliability are garnering significant interest [1–3]. Energy converters are critical components of space nuclear power reactors; they can be categorized as into static (thermocouple converter, alkali metal thermal electric converter and thermionic converter) and dynamic converters (Brayton, Stirling, and Rankine engines) [4]. The free-piston Stirling engine (FPSE) is an efficient converter and has been widely used in aerospace owing to its advantages of high efficiency, reliability, and self-starting ability. Fig. 1 shows a classification of space nuclear power reactors based on their reactor cores and converters; this figure demonstrates that the combination of a heat pipe reactor with a Stirling engine has been investigated extensively in research on space nuclear power reactors since the 2000s. Fig. 2 shows the conceptual design of a space nuclear power reactor in which a heat pipe reactor core is combined with FPSEs.

Fission power is generated in the reactor core, transferred to the heat pipes, and subsequently extracted from the evaporation section of the heat pipe through the shield to the condensation section. It is subsequently transferred to the hot side of the FPSE by a heat exchanger, where waste heat can be discharged to space via a radiator.

The FPSE has been designed and analyzed extensively by companies and institutes since its invention by William Beale in the 1960s. NASA has been developing the FPSE for space applications since the 1980s; NASA Lewis Research Center proposed space power research engines during the SP-100 program and evaluated a linear alternator interaction with various electrical load [5]. The Sunpower Company designed and tested a 1-kW prototype Stirling engine named Re-1000 for NASA, and many reports have been published regarding it [6]; subsequently, the Sunpower Company and NASA Glenn Research Center developed the advanced Stirling radioisotope generator for exploration missions, named ASC-0, ACS-1HS, and FTB, which were tested with different materials and temperatures [7]. In 2010, the Sunpower Company proposed a 12.5-kW FPSE named ASC-E3 for space nuclear power systems [8]. Fan et al. designed a 100-kW FPSE for the lunar surface, and a

* Corresponding author.
** Corresponding author.
E-mail addresses: chlwang@mail.xjtu.edu.cn (C. Wang), dlzhang@mail.xjtu.edu.cn (D. Zhang).

https://doi.org/10.1016/j.net.2020.07.011

Nomenclature:

D	diameter (mm)
A	Area(m^2)
C	coefficient
P	power
l	length (mm)
F	fin
Re	Reynolds number
St	Stanton number
S_d	displacer amplitude
q	flow rate
Bn	Beale number
l	length (mm), leak
W	output power (W)
M	Mass(kg)
V	volume (m^3)
T	temperature (K)
f	friction factor
Z	number of Stirling cylinders
ω	frequency (Hz)
γ	ratio of specific heats (C_p/C_v)
ε	volume compression ratio/efficiency of the regenerator

Subscripts

h	heater, height, convective heat transfer coefficient
id	ideal
ac	actual
fr	friction
c	compression space
r	regenerator
e	expansion space, effective power
k	cooler, thermal conductivity
g	working gas
m	mass
v	velocity
p	piston
l	leak
d	displacer
w	matrix wire, wall
$loss$	heat loss
T	total
cy	cylinder
cp	Inner cylinder
avg	average
s	shuttle
max	maximum
min	minimum

theoretical model was developed for the thermal efficiency prediction of a Stirling cycle [9]. The AMSC Stirling development team is developing a flexure isotope Stirling convertor for high-efficiency radioisotope power systems [10].

Recently, the theoretical analysis of the Stirling engine has been widely conducted. The analysis method for the FPSE can be classified into four categories: the Schmidt, ideal adiabatic analysis, simple analysis, and CFD methods [11]. Ni et al. improved the simple analysis method based on experimental results and proposed an improved simple analysis method [12]. Computational fluid dynamics (CFD) are typically used to simulate the performance of the Stirling engine. Ibrahim simulated a ring heat exchanger in a critical FPSE using CFD-ACE, and the results obtained agreed well with the experimental results [13]. Wilson studied a two-dimensional unidirectional flow heater using CFD to study its pressure drop and mass flow rate [14]. Carlo et al. analyzed heat transfer in a heater using CFD and verified the results experimentally; the calculation results satisfactorily predicted the distribution of velocity and pressure [15]. Mikhael et al. presented a three-dimensional CFD model of the FPSE to characterize the thermal and fluid flow fields during the cycle, and verified the results experimentally; the results showed that regenerator thermal loss

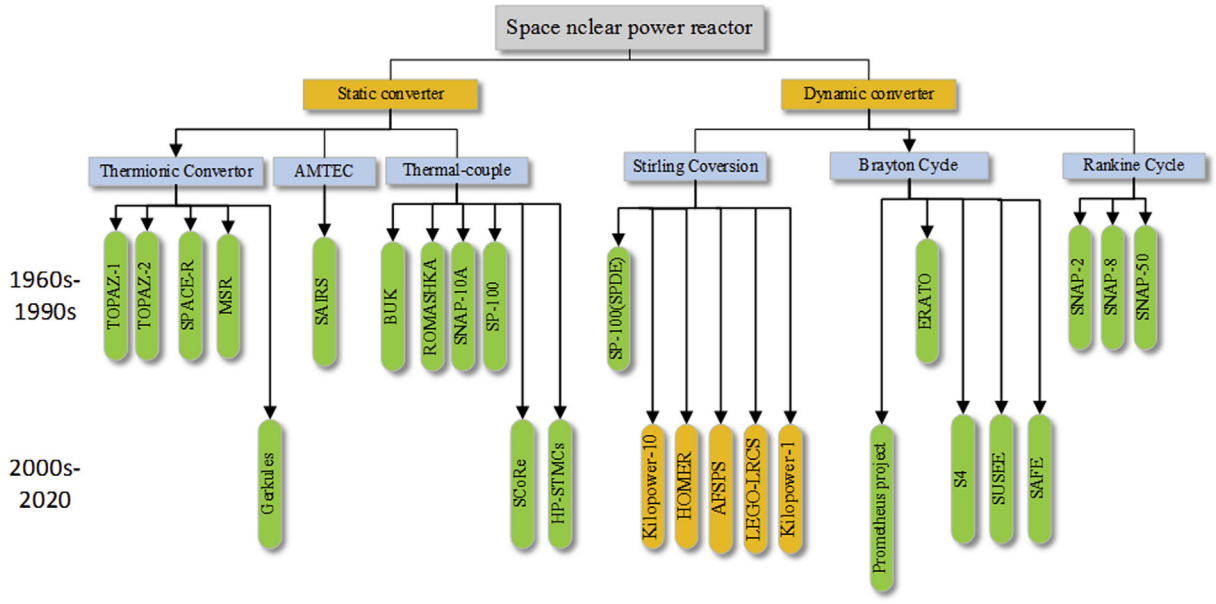

Fig. 1. Classification of space nuclear power reactor.

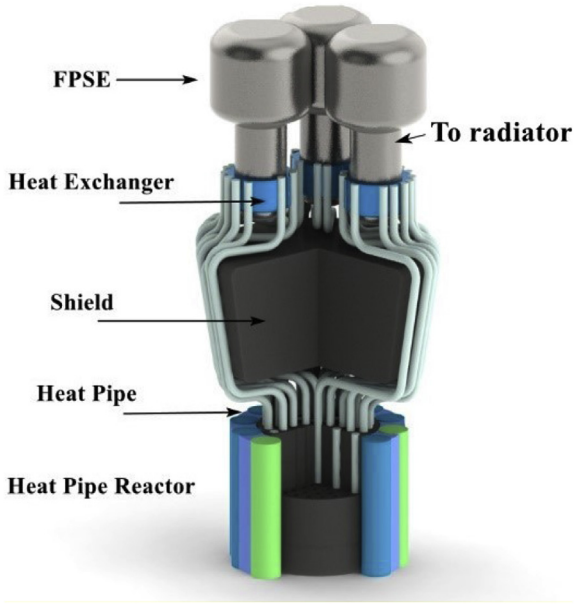

Fig. 2. Conceptual design of space nuclear power reactor.

and pumping power dominated the Stirling engine losses by approximately 9.2% and 7.5%, respectively [16]. Amel et al. investigated the performance of micro and nano metal foam regenerators through a three-dimensional regenerator CFD simulation and found that randomized porous open-cell metal foam made of silver was the optimal structure to fabricate a metal foam regenerator [17]. Buliński et al. developed a CFD model to analyze the effect of the regenerator on performance at different operating conditions for a cold alpha-type Stirling engine [18]. Srinivasa et al. studied the design and structural parameters of mesh-type regenerators in detail; a prototype porous-type Stirling cryocooler regenerator using direct metal laser sintering was studied to improve the performance of the regenerator [19]. Garg et al. investigated the effect of porosity of the regenerator on the performance of a miniature Stirling cryocooler; the results indicated that non-uniform porous matrices reduce power consumption or cool-down time considerably [20].

Although numerous studies have been conducted on the design and analysis of the FPSE, few such engines are suitable for space nuclear reactor power systems. Most of the FPSEs proposed to use a heating tube as the heater or use crank systems to output the power; hence, it is difficult for them to be connected to and used for space nuclear power reactors. Recently, however, an Advanced Stirling Engine (ASE) for aerospace has been considered as trade secrets, design procedures, and structural details for such an engine have been published. In this paper, a 20-kW FPSE is proposed based on the requirements of space nuclear power reactors; furthermore, a code was developed to evaluate the engine's performance based on the improved simple analysis model. This study could provide valuable theoretical support for the design and analysis of the FPSEs for space nuclear power reactors.

2. System description

A schematic of an FPSE combined with a heat pipe reactor is shown in Fig. 3. The heat pipe reactor including reactor fuel, moderator, control drums, reflector and FPSEs are connected to the reactor through alkali heat pipes. Fission heat is generated by the reactor fuel and transferred to the evaporation section of the alkali heat pipe by conduction; subsequently, the heat moves to the condensation section via the liquid metal flow inside the heat pipe. The heat pipe features good isothermal properties; the temperature difference between evaporation and condensation is less than 50 K. A high-conductivity heat exchanger is required to connect the heat pipe with the hot side of the PFSE, whereas waste heat in the cold side of the FPSE can be discharged to space via the cooling loop or radiator.

A typical FPSE primarily contains a heater, cooler, piston, displacer, expansion space, compression space, regenerator, and other structures, such as a pressure shell and support structures. Other structures, such as linear alternators and stator/mover laminations, are used to convert kinetic energy into electrical power. The expansion space is connected to the heater, and the compression space is connected to the cooler. The regenerator is a porous structure between the heater and cooler; the regenerator provides a thermal barrier between heat sources, and it is used to store energy during compression and subsequently return them to the working fluid during expansion. The FPSE operates based on a closed thermodynamic cycle named the Stirling cycle, which is driven by the working gas' expansion in both the heater and expansion space and contraction in both the cooler and compression space. The linear alternator systems are used to convert the movement of the piston to electrical power.

3. System design and analysis

3.1. Requirements analysis

The working gas is critical to the design and analysis of the FPSE. Helium is normally used as the working gas owing to its low viscosity, low density, and high thermal conductivity to improve the performance of the Stirling cycle and decrease the flow resistance inside the FPSE simultaneously. Fig. 4 shows the parameters of space nuclear power reactor that uses a heat pipe reactor according to the system efficiency and coolant temperature at the core outlet; the efficiency of the dynamic converter is much higher than that of the static converter, and the average temperature at the core outlet is approximately 1000 K.

Therefore, a dynamic converter must be designed for space nuclear power reactors; the hot side temperature of the FPSE was set at 1000 K as the average temperature of the core temperature outlet. The classifications of space nuclear power reactor according to the design values of power and specific power are shown in Fig. 5, the specific power decreases with increasing design power, and the range of the space nuclear power reactors that used Stirling engine is from 10 to 100 kW. As the distribution of FPSE is adjusted to reduce the vibration, the number of FPSEs in space nuclear power system is typically 4–8; hence, the design power of the FPSE was selected as 20 kW in this study.

3.2. Numerical model and method

According to basic parameter selection, the concrete parameters of the FPSE can be calculated by the following equations. According to the Schmidt method, the output power P can be written as follows [21]:

$$P = B_n Z \frac{\pi}{8} D_{cy}^2 p_{avg} v_{dm} \tag{1}$$

Where v_{dm} is the average piston speed and $v_{dm} = 2S_d\omega$; Z is the number of Stirling cylinders, equals to 1 in this paper; P_{avg} is the average pressure; B_n is the Beale number written as follows:

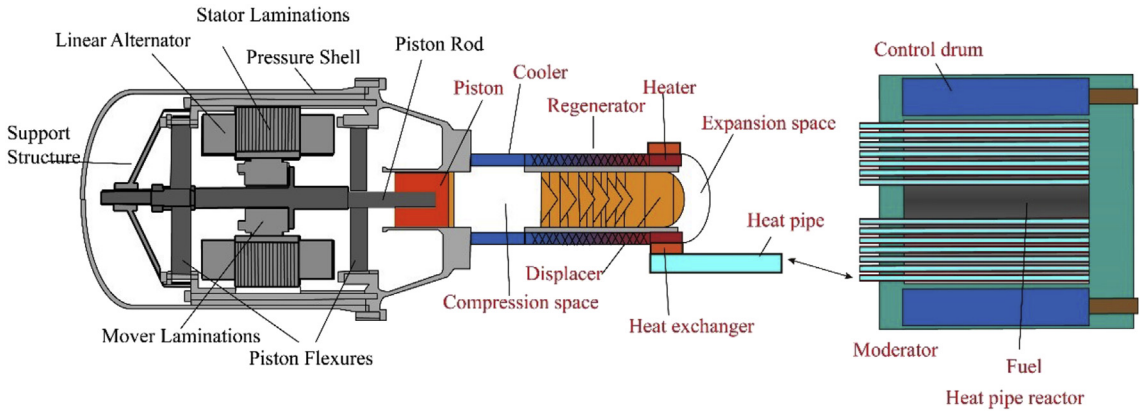

Fig. 3. Schematics of FPSE combined with a heat pipe reactor.

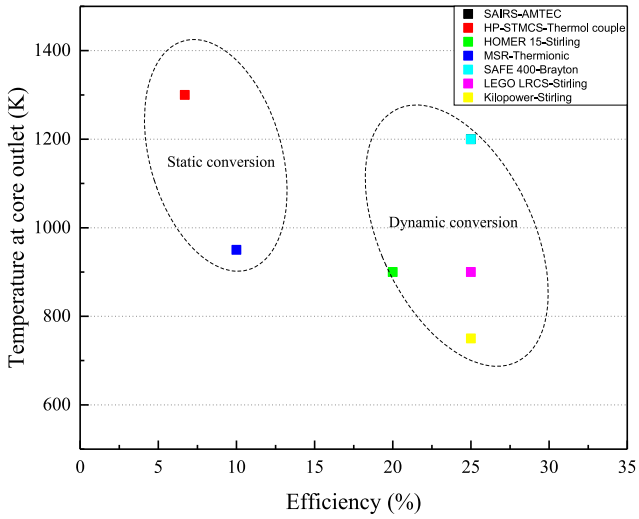

Fig. 4. Parameter of space nuclear power reactor.

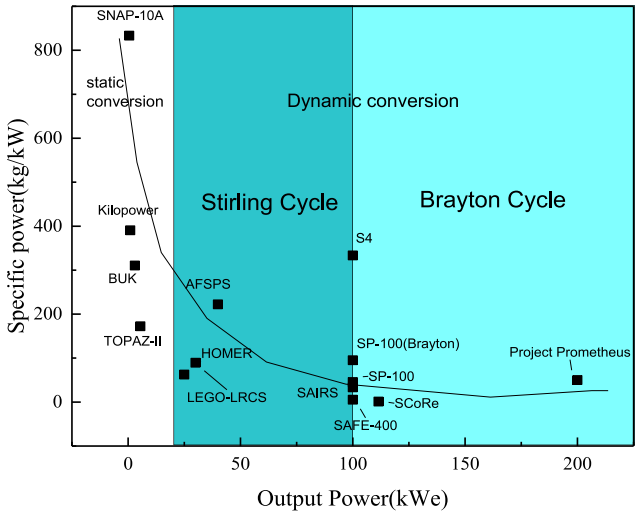

Fig. 5. Classification of space nuclear power reactor.

$$Bn = 0.33\frac{T_E - T_C}{T_E + T_C} \tag{2}$$

The diameter of cylinder D_{cy} can be determined according to eqs. (1) and (2). Subsequently, the swept volume of piston V_p can be calculated as follows:

$$V_p = \frac{1}{4}\pi D_{cy}^2 S_p \tag{3}$$

The total volume V_t in the system contains the volume of compression V_c, the volume of the heater V_h, the volume of the regenerator V_r, the volume of the cooler V_k, and volume of expansion V_e; the total volume V_T can be written as follows:

$$V_T = V_c + V_h + V_r + V_k + V_e \tag{4}$$

The volume compression ratio ε can be written as

$$\varepsilon = \frac{V_{T\max}}{V_{T\min}}, \tag{5}$$

where V_{Tmax} and V_{Tmin} are the total volume changes in one cycle. As it is assumed that the piston and displacer move in sinusoidal motions,

$$V_{T\min} = 0.29V_p + (\chi_h + \chi_r + \chi_k)V_p = (0.29 + \chi)V_p \tag{6}$$

$$V_{T\max} = 1.71V_p + (\chi_h + \chi_r + \chi_k)V_p = (1.71 + \chi)V_p, \tag{7}$$

where $\chi = \chi_h + \chi_r + \chi_k$. According to eqs. (5)–(7), V_t can be written as follows:

$$V_t = \chi V_P \tag{8}$$

According to the volume distribution in each part, the basic parameter of the FPSE can be determined. Furthermore, the V_y can be calculated as follows [22]:

$$\frac{V_p}{V_d} = \left\{\left[(0.11(1+\zeta)T_H/T_K)\Big/\left(1+3400\left(\frac{T_H}{T_K}-1\right)\Big/\beta\right.\right.$$
$$\left.\left.-0.02\left(\frac{T_H}{T_K}-1\right)(\beta T_K/T_H)0.5\right)\right]^{0.5} + f_\zeta + f_\beta + f_\delta\right\} \tag{9}$$

where

$$f_\zeta = 0.357\zeta - 0.78 \tag{10}$$

Table 1
Equations for the ideal adiabatic model.

$p = MR/(V_c/T_c + V_k/T_k + V_r/T_r + V_h/T_h + V_e/T_e)$	pressure
$dp = \frac{-\gamma p(dV_c/T_{ck} + dV_e/T_{he})}{V_c/T_{ck} + \gamma(V_k/T_k + V_r/T_r + V_h/T_h) + V_e/T_{he}}$	
$m_c = pV_c/(RT_c)$	mass
$m_k = pV_k/(RT_k)$	
$m_r = pV_r/(RT_r)$	
$m_h = pV_h/(RT_h)$	
$m_e = pV_e/(RT_e)$	
$dm_c = (pdV_c + V_c dp/\gamma)/(RT_{ck})$	Mass accumulation
$dm_e = (pdV_e + V_e dp/\gamma)/(RT_{he})$	
$dm_k = m_k dp/p$	
$dm_r = m_r dp/p$	
$dm_h = m_h dp/p$	
$\dot{m}_{ck} = -dm_c$	Mass flow
$\dot{m}_{kr} = \dot{m}_{ck} - dm_k$	
$\dot{m}_{he} = dm_e$	
$\dot{m}_{rh} = \dot{m}_{he} + dm_h$	
$T_{kr} = T_k$	Conditional temperature
$T_{rh} = T_h$	(Temperature of the
$if\ \dot{m}_{ck} > 0, T_{ck} = T_c, else T_{ck} = T_k$	working gas changed
$if\ \dot{m}_{he} > 0, T_{he} = T_h, else T_{he} = T_e$	with the flow direction)
$dT_c = T_c(dp/p + dV_c/V_c - dm_c/m_c)$	temperature
$dT_e = T_e(dp/p + dV_e/V_e - dm_e/m_e)$	
$dQ_k = V_k dpc_v/R - c_p(T_{ck}\dot{m}_{ck} - T_{kr}\dot{m}_{kr})$	Energy
$dQ_r = V_r dpc_v/R - c_p(T_{kr}\dot{m}_{kr} - T_{rh}\dot{m}_{rh})$	
$dQ_h = V_h dpc_v/R - c_p(T_{rh}\dot{m}_{rh} - T_{he}\dot{m}_{he})$	
$dW_c = pdV_c\ dW_e = pdV_e\ dW = dW_e + dW_c$	

$$f_\beta = 0.525 - 8.8 \times 10^{-5}\beta \tag{11}$$

$$f_\delta = 0.548\frac{T_H}{T_K} - 0.54 \tag{12}$$

$$\zeta = (V_{KD} + V_{HD}T_K/T_H + V_{RD}T_K/T_R)/V_y \tag{13}$$

$$\beta = \frac{p_m \omega V_y^2}{RT_K \mu_{GC} A_C^2} \tag{14}$$

According to eq. (7), the swept volume of the displacer V_d can be calculated. Therefore, the displacer amplitude S_d can be written as:

$$S_d = \frac{V_d}{\pi\left(\frac{D_{cp}}{2}\right)^2} \tag{15}$$

Eqs. (1)–(13) can calculate the basic parameters of an FPSE. However, the output power must be evaluated to determine if it can satisfy the design value; hence, the temperature and mass flow rate at the inlet of the heater must be determined. As the movements of the piston and displacer are sinusoidal, the volumes of compression space V_e and expansion space V_c changed with time can be expressed as:

$$V_e(t) = \frac{1}{2}V_e(1 + \cos\omega t) \tag{16}$$

$$V_c(t) = \frac{1}{2}V_e(1 - \cos\omega t) + \frac{1}{2}\frac{V_e}{V_c}\left[1 + \cos(\omega t + \alpha_p)\right], \tag{17}$$

Where V_e and V_c are the swept volumes of the expansion space (V_e) and compression space (V_c), respectively. It is assumed that the pressure in each part is the same at the same time t. Therefore, the total mass of the working gas (M_T) can be written as follows:

$$M_T = \frac{p(t)V_e}{RT_e(t)} + \frac{p(t)V_c}{RT_c(t)} + \frac{p(t)V_r}{RT_r(t)} + \frac{p(t)V_h}{RT_h(t)} + \frac{p(t)V_k}{RT_k(t)}, \tag{18}$$

Where T_R is the temperature of the regenerator:

$$T_r = \frac{(T_e - T_c)}{\ln(T_e/T_c)} \tag{19}$$

. Table 1 presents the equations for the ideal adiabatic model. The ideal adiabatic analysis is primarily based on the following assumptions: a) The compression and expansion processes are adiabatic. b) Gas leakage and pressure drops are nonexistent. c) The temperatures in the heater and cooler are constant. d) The regenerator is perfect. e) The working gas is an ideal gas. The calculation of the ideal adiabatic analysis model is higher than the real situation of the FPSE, and energy loss needs to be considered to modify the model. Eqs. (16)–(19) was placed into the differential equations using for ideal adiabatic analysis, which were solved. When the ideal Stirling cycle is obtained, then the heat loss must be calculated as following:

The improved simple analysis method was used to analyze and evaluate the working condition of the FPSE in detail; experimental results verified that the method could be used to precisely analyze the performance of the FPSE. The heat loss primarily involves six parts: a) regenerator heat transfer loss, b) flow resistance loss, c) regenerator heat transfer loss, d) gas spring hysteresis power loss, e) shuttle heat loss in the displacer, and f) heat conductivity loss in the pressure shell. The gas spring hysteresis power loss was neglected in this paper, as the value is very small compared with the other loss. The heat loss can be calculated using the following equations. The temperature difference between the wire and helium cannot be neglected for a non-ideal regenerator, and the heat loss in the regenerator can be written as follows:

$$Q_{rloss} = Q_r(1 - \varepsilon), \tag{20}$$

Where ε is the efficiency of the regenerator, expressed as

$$\varepsilon = \frac{\frac{1}{2}StA_{wg}\Big/A}{1 + \frac{1}{2}StA_{wg}\Big/A}, \tag{21}$$

Where A_{wg} is the internal wetted area in the regenerator and St is the Stanton number expressed as follows:

$$St = 0.46\mathrm{Re}^{-0.4}\mathrm{Pr}^{-1} \tag{22}$$

The flow resistance power loss in the heater, regenerator, and cooler can be calculated using the following formula:

$$\Delta p = -\frac{2C_{fr}\mu_g\rho_g u_g V}{Ad^2}, \tag{23}$$

Where C_{rf} is the friction factor. The flow resistance power can be calculated in one cycle as follows:

$$W_{fr} = \int_0^{2\pi}\left(\Delta p\frac{\partial V}{\partial\theta}\right)d\theta \tag{24}$$

Shuttle heat loss of the displacer. The displacer generates some heat from the hot chamber to the cold chamber during oscillation. This means that the heater should absorb more heat:

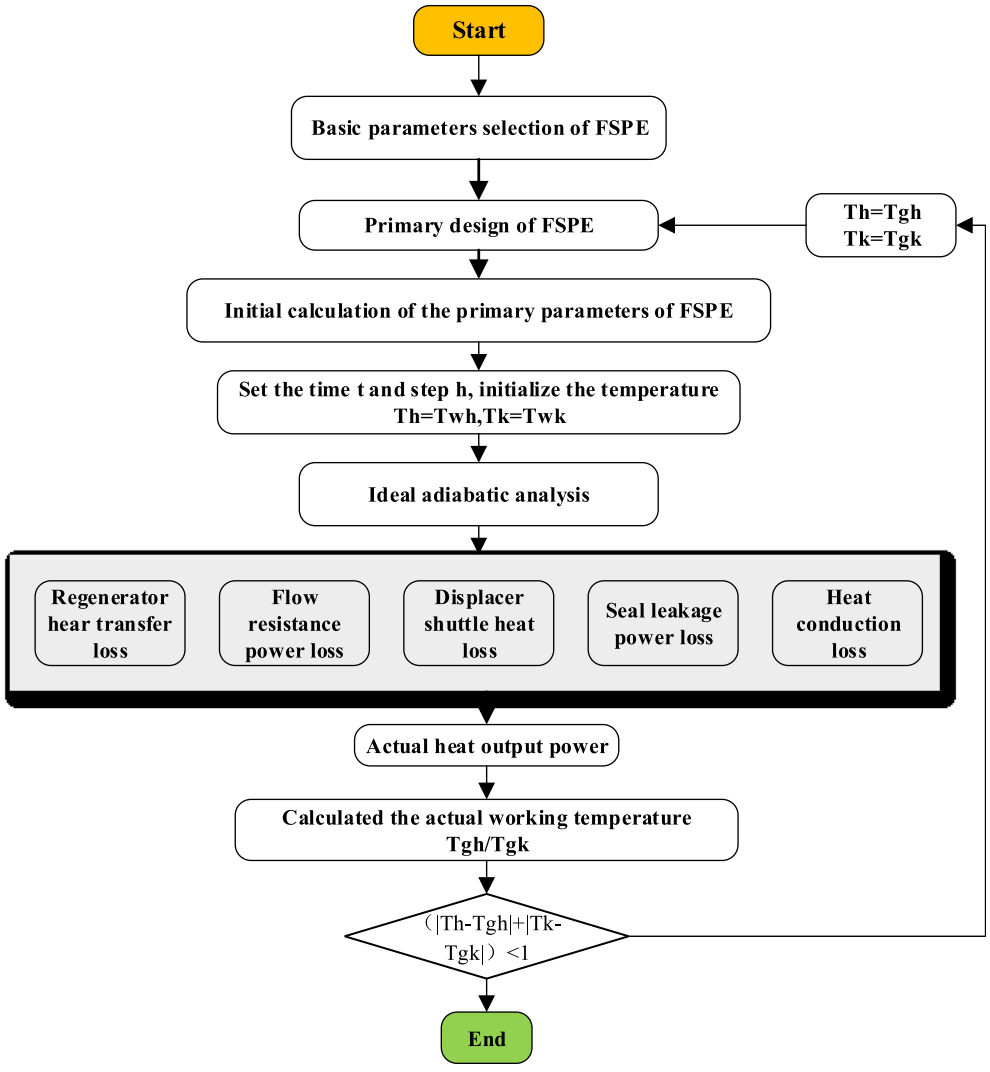

Fig. 6. Program flow diagram.

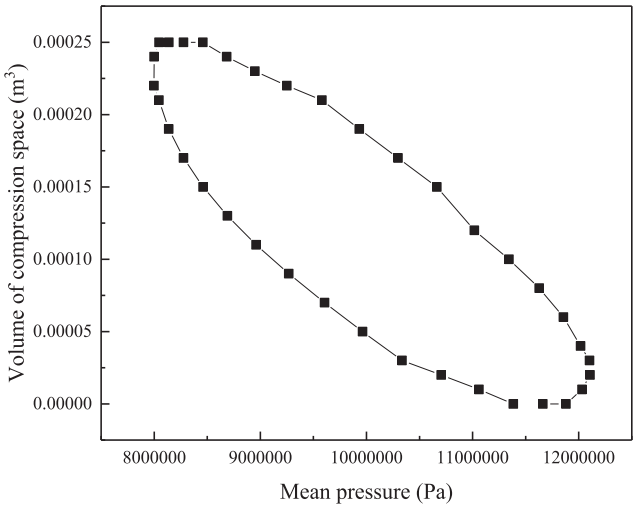

Fig. 7. P–V diagram of the mean pressure and compression space.

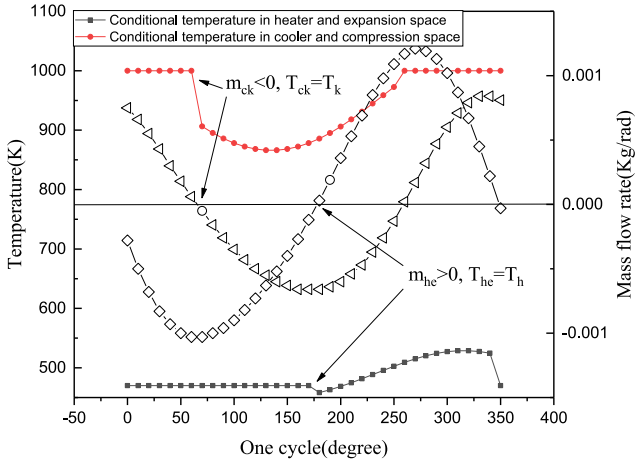

Fig. 8. Conditional temperature changes in one cycle.

$$Q_{sh}=\frac{\pi}{6}\frac{S_p^2 k_g (T_h-T_k)D_{cy}^2}{\delta L_p}\left(\frac{1+\lambda}{1+\lambda^2}\right), \tag{25}$$

Where $\lambda$is expressed as

$$\lambda=1+\frac{k_g}{2\pi\delta}\left(\frac{L_{tc}}{k_{mc}}+\frac{L_{tp}}{k_{mp}}\right) \tag{26}$$

Seal leakage power loss. Leakage mass flow pasted with a sealing ring can be regarded as incompressible clearance flow; mass leakage affects the total mass of the working gas and decreases the output power of the engine. The pressure difference between the ends of the displacer is negligible compared with the pressure difference between the ends of the power piston. Hence it can be neglected in the calculation.

$$W_l=q_{ml}\cdot c_p\cdot T_l, \tag{27}$$

Heat conduction loss in the engine primarily involves two parts, including heat conduction in the cylinder of pressure shell and displacer heat conduction loss, which can be evaluated according to the Fourier law:

$$Q_w=\frac{k_w A_w (T_h-T_k)}{l} \tag{28}$$

According to the calculation of the FPSE, the total power and basic movement of the piston and displacer can be determined.

$$Q_{ach}=Q_{idh}+Q_w+Q_{rloss}+Q_{sh} \tag{29}$$

$$Q_{acco}=Q_{adco}+Q_w+Q_{rloss}+Q_{sh}+W_{fr}+W_l \tag{30}$$

$$W_{acip}=W_{adip}-W_{fr}-W_l, \tag{31}$$

Where Q_{ach} is the actual heat inlet of the heater, Q_{idh} the ideal heat inlet of the heater, Q_{acco} the actual heat outlet of the cooler, Q_{adco} the ideal heat outlet of cooler, W_{acip} the actual output power, and W_{adip} the ideal output power. The actual temperatures in the heater T_{gh} and cooler T_{gk} can be calculated as follows:

$$T_{gh}=T_{wh}-\frac{Q_{ach}}{hA_h} \tag{32}$$

$$T_{gk}=T_{wk}-\frac{Q_{acco}}{hA_{co}} \tag{33}$$

Where A_h and A_{co} is the convective heat transfer coefficient of heater and cooler, respectively.

3.3. Solution procedure

A code was developed to analyze the performance of the FPSE. Fig. 6 illustrates the program flow diagram of the code in this study. In the first step, the basic parameter of the FPSE was selected according to the requirements of space nuclear power reactors, where the primary parameters were calculated according to eqs. (16)–(19). The temperatures in the expansion and compression space were assumed, and the movement in one Stirling cycle was discretized into 36 (every 10°) in the program to solve the ideal adiabatic model. In the second step, the performance of the proposed FPSE was analyzed using the ideal adiabatic method, followed by a heat loss analysis. The ideal adiabatic model in Table 1 can be calculated using the fourth-order Runge–Kutta method, as follows:

$$\begin{cases} y_{j,i+1}=yj,i+\frac{1}{6}(K_{j1}+2K_{j2}+2K_{j3}+K_{j4}), \\ K_{j1}=hf_i(x_i;y_{1i},y_{2i},\cdots y_{ni}), \\ K_{j2}=hf_j\left(x_i+\frac{h}{2};y_{1i}+\frac{K_{11}}{2},y_{2i}+\frac{K_{21}}{2},\cdots,y_{ni}+\frac{K_{n1}}{2}\right), j=1,2,\cdots,n \\ K_{j3}=hf_j\left(x_i+\frac{h}{2};y_{1i}+\frac{K_{12}}{2},y_{2i}+\frac{K_{22}}{2},\cdots,y_{ni}+\frac{K_{n2}}{2}\right), \\ K_{j4}=hf_j(x_i+h;y_{1i}+K_{13},y_{i2}+K_{23},\cdots,y_{ni}+K_{n3}) \end{cases} \tag{34}$$

In the third step, the heat loss in the FPSE must be considered based on the ideal adiabatic model, including regenerator heat loss, gas spring hysteresis power loss, flow resistance power loss, displacer shuttle heat loss, seal leakage power loss and heat conduction loss. After the third step, the temperature in the expansion and compression space can be calculated, and the iterative calculation is stopped when the temperature satisfies the condition of convergence.

4. Results and discussion

4.1. Verification and validation

The design and analysis procedure was validated by comparing the simulation results with an ideal Stirling engine. The pressure-volume (P–V) diagram of the mean pressure and compression space is shown in Fig. 7. The piston motion in the ideal Stirling cycle is discontinuous, while that in the proposed Stirling engine is continuous; therefore, no turning point exists in the Stirling cycle, which is shown as a continuous circle in the P–V diagram. Fig. 8 illustrates the temperature changes of helium in one cycle; as shown, the conditional temperature changes when the mass flow rate is reversed in each part. The code results satisfied the equations and actual situations of the Stirling engine.

For the validation of the model, the output power and temperature calculation results were compared with the experimental results from RE-1000 [24]. The main parameters of the RE-1000 are shown in Table 2. Table 3a shows the comparison between the experimental and code calculation results. As shown, the results by the present code agree reasonably well with the experimental results, with a maximum relative error of 17.1% for the output power; this may be because an external heating tube was used as the heater in RE-1000, and hence the estimated heat loss was not

Table 2
Main parameters of RE-1000 in the test.

Parameters	value
Area of piston (cm^2)	25.679
Area of displacer (cm^2)	25.25
Area of displacer rod (cm^2)	2.16
Volume of heater (cm^3)	27.4
Volume of cooler (cm^3)	20.42
Volume of regenerator (cm^3)	56.1
Hot side temperature (K)	873
Cold side temperature (K)	297.25
Number of heat tubes	34
Length of heater (cm)	18.34
Length of cooler (cm)	7.92
Length of regenerator (cm)	6.4
Porosity of wire (%)	81.2
Diameter of the wire (mm)	0.0889
Mean pressure (MPa)	7
Frequency (Hz)	30

Table 3a
Experimental results and calculation results by the code.

Parameter	RE-1000 [24]	Code calculation	Error
Indicate power (W)	739	866	17.1%
Temperature at expansion space (K)	839	848	1.1%
Temperature at compression space (K)	318	326	2.5%
Mean pressure	7 MPa	7 MPa	–

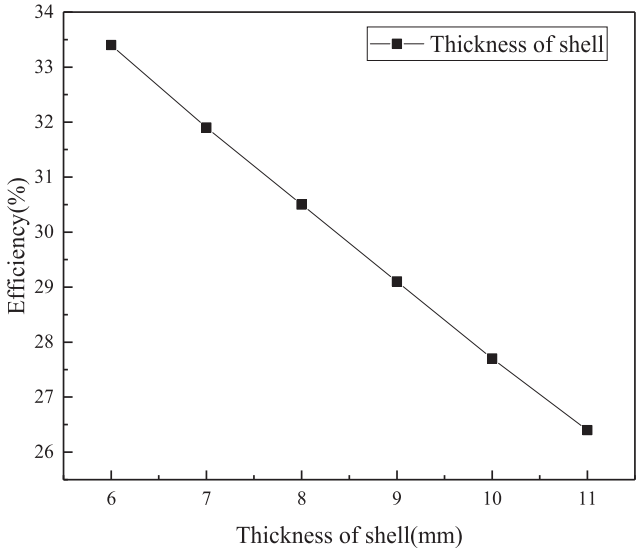

Fig. 9. Effect of shell thickness on system efficiency.

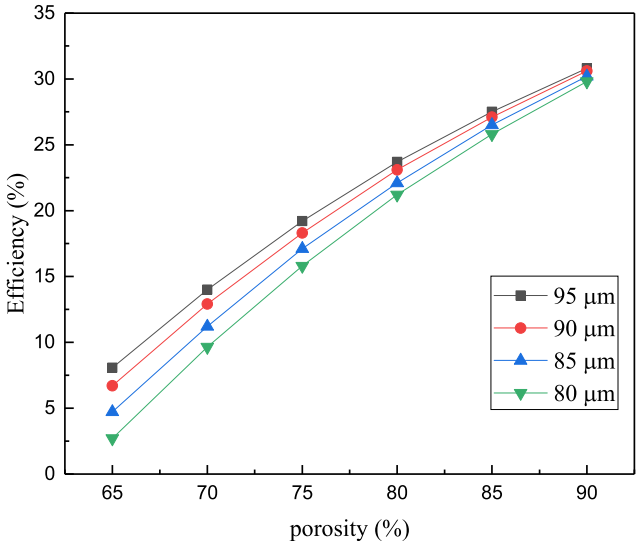

Fig. 11. Effects of porosity and diameter of wire on system efficiency.

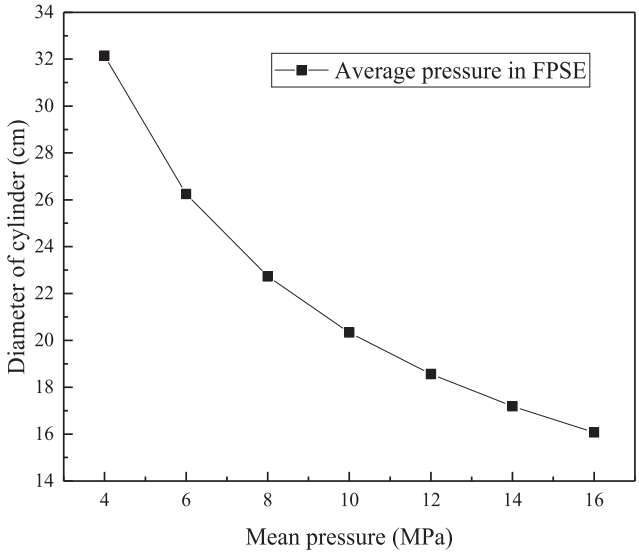

Fig. 10. Effect of mean pressure on diameter of the cylinder.

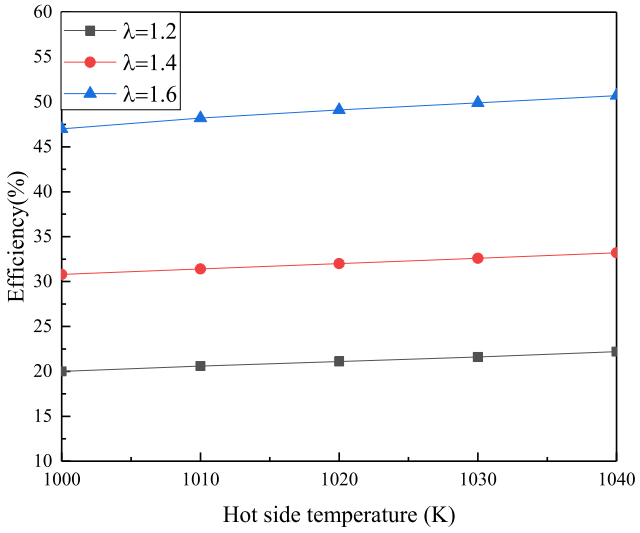

Fig. 12. Effects of hot side temperature and compression ratio on system efficiency.

accurate. The verification and validation results proved the efficacy of the developed code for the design and analysis of the FPSE.

4.2. Effect of structure parameters

The effect of the thickness shell on the system efficiency is illustrated in Fig. 9. As shown, when the thickness of the pressure shell increased, the system efficiency decreased linearly. The thickness of the pressure shell is critical in the system efficiency because the heat conduction loss is a major contributor to the total heat loss. Therefore, an appropriate reduction in pressure shell thickness can improve the power output significantly; however, the thickness is determined by the mean pressure and material of the shell. In this study, the thickness of the pressure shell is selected as 8 mm according to the principle of pressure shell design (for stainless steel).

Fig. 10 shows the effect of mean pressure on the diameter of the cylinder; the structure of the FPSE is more compact with the mean pressure increased at the same output power. However, the leakage

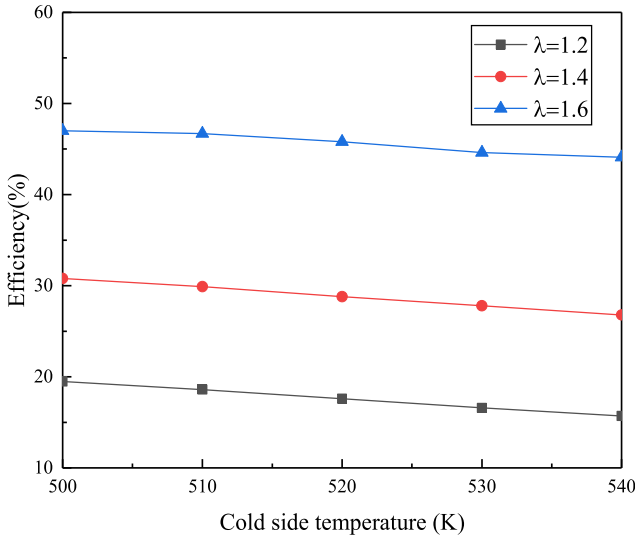

Fig. 13. Effects of cold side temperature and compression ratio on system efficiency.

Table 3b
Main parameters of FPSE.

parameter	value
Design power (W)	20,000
Average pressure (MPa)	10
Efficiency (%)	30.6
Frequency (Hz)	70
Displacer phase angle (°)	90
Beale number	0.11
Volume compression ratio ε	1.4
Heater/Cooler/regenerator tube outside diameter (mm)	20
Length of heater (mm)	50
Length of cooler (mm)	50
Length of regenerator (mm)	100
Porosity of wire (%)	80
Swept volume of piston V_p (cm^3)	251.2
Swept volume of displacer V_d (cm^3)	313.75
Volume of heater (cm^3)	200
Volume of cooler (cm^3)	200
Volume of regenerator (cm^3)	420
S_p (mm)	8
S_d (mm)	10
Area of displacer (cm^2)	254.34
Area of piston (cm^2)	254.34
Hot side temperature (K)	1000
Cold side temperature (K)	500
Material of shell	Stainless steel
Thickness of the pressure shell (mm)	8

of the working gas is more serious with the increased mean pressure, which increased the thickness of the pressure shell and the heat conduction loss but decreased the system efficiency simultaneously. Typically, the mean pressure of the FPSE for space nuclear power reactors is from 5 to 15 MPa; therefore, the mean pressure was select as 10 MPa considering the risk of helium leakage.

The effects of wire porosity and diameter on system efficiency are shown in Fig. 11; the lines represent wires of different diameters with porosity ranging from 65% to 90% that filled the regenerator; the system efficiency increases with the wire diameter. Porosity is critical to the system efficiency; the system efficiency increased with the wire porosity because the regenerator improved the performance of helium when it returned from the cooler to the heater. However, the growth for system efficiency declined when the wire porosity was higher than 80%; this was because the wire diameter could affect the hydraulic diameter of the regenerator, which could increase the flow resistance.

4.3. Effects of hot side and cold side temperatures

During the requirements analysis for space nuclear power reactors, the temperature of 1000 K was considered for the hot side temperature of the heater, while 500 K was considered for the cold side temperature. The temperature of the hot side can be changed owing to the thermal power changes of the reactor core, whereas the temperature of the cold side can be changed as the performance of the radiation system changes. The effects of the hot side temperature and compression ratio on the system efficiency are illustrated in Fig. 12. As shown, the system efficiency increases linearly with the hot side temperature. Fig. 13 shows the effect of the cold side temperature and compression ratio on the system efficiency. It indicates that the system efficiency decreased slightly when the cold side temperature increased, and the system efficiency increased with the compression ratio.

The compression ratio ε significantly affected the system efficiency; the compression ratio increased by 16.7%, while the system efficiency increased by 42%. However, a higher compression ratio could be limited by practical applications. It was difficult to reach a high compression ratio in a real Stirling engine; a compression ratio above 2 is unrealistic for the FPSE. Hence, the compression ratio was set to 1.4 in this study. The final parameters of the proposed FPSE are shown in Table 3b. According to the analysis of the code, the output power was 2.1 kW, which was within the design requirements.

5. Conclusion

In this paper, a 20-kW FPSE was proposed by analyzing the requirements of space nuclear power reactors. A code was developed based on the improved simple analysis method to evaluate the performance of the proposed FPSE, which was solved using the fourth-order Runge–Kutta method. The results showed that the simulated output power was 21 kW, which satisfied the design requirements. The conclusions are summarized as follows:

1. For the code's verification and validation, the code results satisfied the actual situation of the Stirling engine in a period. The model results were benchmarked with the experimental data from RE-1000, and the maximum relative error was 17.1%, indicating the fidelity and reasonability of the developed code.
2. System efficiency increased as the thickness of the pressure shell decreased. The porosity of the wire in the regenerator was critical to the system efficiency; the system efficiency increased with the porosity, while the growth of the system efficiency declined when the wire porosity was higher than 80%.
3. The system efficiency increased with the compression ratio; the compression ratio increased by 16.7%, while the system efficiency increased by 42%. Furthermore, system efficiency changed linearly with the temperature changes at the cold and hot sides.

Declaration of competing interest

The authors declare that they have no known competing financial interests or personal relationships that could have appeared to influence the work reported in this paper.

Acknowledgement

The authors would like to thank the support from the National Key Research and Development Program of China (No.

2019YFB1901300), National Natural Science Foundation of China (No. 11675162).

Appendix A. Supplementary data

Supplementary data to this article can be found online at https://doi.org/10.1016/j.net.2020.07.011.

References

[1] Weichao Li, et al., Investigation on steam contact condensation injected vertically at low mass flux: Part I pure steam experiment, Int. J. Heat Mass Tran. 131 (2019) 301–312.
[2] Weichao Li, et al., Investigation on thermal stratification induced by steam-air mixture vertical injection with shallow submergence depth, Prog. Nucl. Energy 115 (2019) 52–61.
[3] Weichao Li, et al., Experimental investigation on thermal stratification induced by steam direct contact condensation with non-condensable gas, Appl. Therm. Eng. 154 (2019) 628–636.
[4] Zhiwen Dai, et al., Thermoelectric characteristics analysis of thermionic space nuclear power reactor, Int. J. Energy Res. 4 (2019), https://doi.org/10.1002/er.4926.
[5] G. Dochat, SPDE/SPRE Final Summary Report, NASA Contractor Report, 1993.
[6] J.G. Schreiber, RE-1000 Free-Piston Stirling Engine Update, ENERGY PRODUCTION AND CONVERSION, 1985.
[7] J.G.W. Jack Chan, Jeffrey G. Schreiber, Development of Advanced Stirling Radioisotope Generator for Space Exploration, American Institute of Physics, 2007.
[8] W. Wong, et al., Pathfinding the Flight Advanced Stirling Convertor Design with the ASC-E3, 2012.
[9] S. Fan, et al., Thermodynamic analysis and optimization of a Stirling cycle for lunar surface nuclear power system, Appl. Therm. Eng. 111 (2017) 60–67.
[10] M.W. Michael Amato, Glenn Driscoll, Allen Peterson, Joseph VanderVeer, Robert Sievers, FLEXURE ISOTOPE STIRLING CONVERTOR (FISC) DEVELOPMENT PROGRESS.", NETS, 2019.
[11] R.W. Dyson, et al., Review of computational stirling analysis methods, AIAA J. (2004), 5582, https://doi.org/10.2514/6.2004-5582.
[12] M. Ni, et al., Improved simple analytical model and experimental study of a 100W β-type stirling engine, Appl. Energy 169 (2016) 768–787.
[13] M.B. I.a.M. Mittal, A 2-D CFD model of a free piston stirling engine for space applications with annular heat exchangers, AIAA (2004), 5583, https://doi.org/10.2514/6.2004-5583.
[14] S. Wilson, et al., Experimental and computational analysis of unidirectional flow through stirling engine heater head, AIAA, 2005, 5539.
[15] M. Carlo, F.R. Bartolini, A numerical method to EVALUAE heat exchangers performance OF external combustion engine, IEEE 5 (1989) 2591–2596, https://doi.org/10.1109/IECEC.1989.74840.
[16] N.N. Mikhael, M. E.-G., S.A. El-Ghafour, CFD simulation and losses analysis of a beta-type stirling engine, PORT SAID ENGINEERING RESEARCH JOURNAL 22 (2) (2018) 85–101, https://doi.org/10.21608/pserj.2018.32106.
[17] A. Najafi Amel, et al., Study the heat recovery performance of micro and nano metfoam regenerators in alpha type stirling engine conditions, Nanoscale Microscale Thermophys. Eng. 22 (2) (2018) 137–141.
[18] Z. Buliński, et al., A Computational Fluid Dynamics analysis of the influence of the regenerator on the performance of the cold Stirling engine at different working conditions, Energy Convers. Manag. 195 (2019) 125–138.
[19] K.V. Srinivasan, et al., Design and development of porous regenerator for Stirling cryocooler using additive manufacturing, Thermal Science and Engineering Progress 11 (2019) 195–203.
[20] S.K. Garg, et al., Effect of Porosity of the regenerator on the performance of a miniature Stirling cryocooler, Thermal Science and Engineering Progress 15 (2020) 100442.
[21] Z.Z. Guozhu Qian, Shanqing Yan, Principle and Design of Stirling Engine, 1987.
[22] M. Salvatore, G.M.B. Oriti, Advanced Stirling Convertor Testing at NASA Glenn Research Center, AIAA, 2007.
[24] J.G. Schreiber, S.M. Geng, G.V. Lorenz, RE-1000 Free-Piston Stirling Engine Sensitivity Test results. Final Report. United States: N. P., 1986, https://doi.org/10.2172/532524. Web.